Korean J. Chem. Eng., **27**(6), 1646-1653 (2010)
DOI: 10.1007/s11814-010-0268-6

A numerical study of two-phase transonic steam flow through convergence-divergence nozzles with different rates of expansion

Behnam Nikkhahi, Mehrzad Shams†, and Masoud Ziabasharhagh

Faculty of Mech. Engineering, K.N.Toosi University of Technology, Tehran, Iran
(*Received 10 December 2009 • accepted 13 February 2010*)

Abstract−During transonic flow of steam in divergence nozzles, flow first supercools and then nucleates to become two-phase droplet flow. This phenomenon especially occurs in the last stages of steam turbines and affects performance. In this research, a numerical scheme for two-phase flow in nozzle passages is developed. An Eulerian-Eulerian reference frame is used for both phases. The shear stress transport turbulence model is used to model the Reynolds stresses appearing in the averaged Navier-Stokes equations. The homogeneous nucleation model is applied for the mass transfer in the transonic conditions. In this paper three nozzles with different rate of expansion are employed to be under study. Overall pressure ratio (static to total pressure) and droplet size are compared with the experimental data and good agreements are observed.

Key words: Nucleation, Two-phase Flow, Nozzles, CFD, Eulerian-Eulerian

INTRODUCTION

Nucleation in flowing steam has traditionally been studied because of its industrial importance, especially steam turbines as the low pressure cases and nuclear reactors as the high pressure. During the expansion of steam, the state crosses the saturation line and the fluid first supercools and then nucleates to become a two-phase mixture consisting of a large number of fine droplets which are carried by the vapor. In these situations the system leaves the thermodynamic equilibrium and release of latent heat causes the flow return to equilibrium. Nucleation through the steam has been widely under studied as the cases of high and low pressure in several years. Many experimental, theoretical and numerical investigations into the behavior of wet steam in turbines and nozzles have been reported. Bakhtar and Zidi [1] studied the nucleation phenomena in 2-D flowing high-pressure steam in three nozzles with different rates of expansion experimentally and recorded the pressure ratio and droplet size at the axial line [1]. They continued their studies theoretically within these nozzles [2]. Gerber et al. [3] developed a numerical model based on Eulerian-Lagrangian approach for two-phase steam flow [3]. They compared their results of low-pressure convergence-divergence nozzles with Moore et al. (1973) and observed good correspondence. Gerber and Kermnai [4] presented an Eulerian-Eulerian multi phase method for non-equilibrium condensation in transonic steam flow [4], and used it for low and high-pressure tests in nozzles and met good agreement in comparison with Moore (1973) and Bakhtar's [2] experimental results. Numerical calculation for two-phase steam flow, using a Jameson-style finite volume method on an unstructured and adaptive triangular mesh was presented by Simpson and White in 2005 [5]. This approach has been applied for both steady and unsteady problems. In the presented research, an Eulerian-Eulerian approach is applied for numerical study of high-pressure two-phase steam flow within three nozzles with different rate of expansion. The results are shown as overall (static to total) pressure, Mach number, Water mass fraction, droplet size and droplet number profiles and water mass fraction contours. For each nozzle, in the same pressure condition of each test, a simulation of dry steam is presented. Also, overall pressure and Mach number profiles of wet and dry steam are compared. Fig. 1 shows the divergence part geometries of these three nozzles.

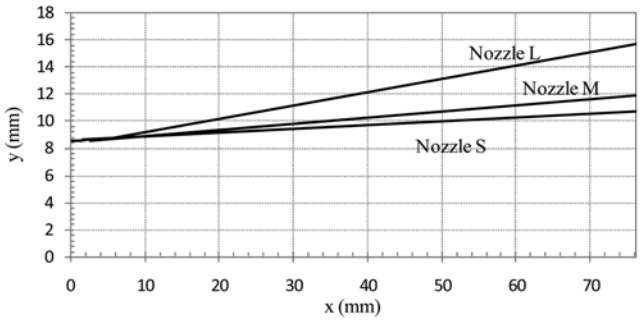

Fig. 1. Nozzles geometries.

NUMERICAL STRATEGY, GOVERNING EQUATIONS AND ASSUMPTIONS

In this study, Navier-Stokes viscous flow solution, with employing a pressure-based finite volume discretization is applied. Method of Eulerian-Eulerian is governing both steam and droplet phases. The second phase appears with the submicron droplet during the nucleation. Within the high level supercooling of steam flow (depending on expansion rate), numerous drops could be appear. After that expansion of flow and decreasing the enthalpy and temperature, homogeneous nucleation in condensing steam occurs at adequate levels of supercooling. The level of supercooling is the difference between the local vapor temperature and the saturation temperature.

†To whom correspondence should be addressed.
E-mail: shams@kntu.ac.ir

This matter is typically 30-50 K for low pressure steam. In this condition mass and heat transfer bring the flow near the equilibrium. Phase change occurs at high vapor velocities and high expansion rates. The available droplet surface area necessary to bring or maintain the flow at near thermodynamic equilibrium must come from a fine mist of droplets formed by homogeneous nucleation [3].

Assumptions for condensing steam flow are in this order: the droplets have very small travel at the vapor phase velocity that applies only to the mean velocity field, while instantaneous velocity components of the phase differ. This assumption eliminates the calculation of momentum equation for the second phase. The droplets in the flow do not appear at high mass fraction, and therefore the volume occupied by the liquid can be neglected. Since the droplets are very small, their temperature is assumed uniform through the droplets and can be determined by capillarity conditions [4]. For modeling the thermodynamics properties of water and steam and surface tension of water in numerical solution, the equations of IAPWS (International Association of Properties of Water and Steam) are applied [6,7].

1. Continuity Equations

Mass conservation equations for gas phase with source term of S_m, is

$$\frac{\partial}{\partial x_j}(\rho_g u_j(1-\alpha)) = S_m \tag{1}$$

Where ρ_g stands for density of vapor phase, α represents the mass fraction (α=m_f/m_{total}) and the mass source of S_m, is defined to reflect the condensation and vaporization processes. In the case of evaporation, the mass source of S_m is positive while it is negative for the condensation. The continuity equation for droplet phase with the source term of S_α that determined the condensation rate of vapor can be shown as below:

$$\frac{\partial}{\partial x_j}(\rho_l u_{g_j}\alpha) = S_\alpha \tag{2}$$

where ρ_l is the density of liquid. From the definition of S_m and S_α, it is clear that they are equal and opposite to each other. These scalars are obtained by considering the mass growth rate of a droplet of size $\bar{r}$. These sources terms with unit of [kg/m^3 s] are defined as [3];

$$S_m = -S_\alpha = -\rho_l N(4\pi\bar{r}^2)\frac{dr}{dt}\rho_g \tag{3}$$

where N is the number of droplets per unit mass of vapor ([#/m_g]) and term of ($4\pi\bar{r}^2$) is the average interfacial surface area of a single droplet. is the sum of the interfacial surface areas per unit mass of the vapor.

2. Momentum Equations

The vapor momentum equations are based on the Reynolds averaged Navier-Stokes equations for turbulent flow and the shear stress transport model for the turbulent Reynolds stress terms. Momentum conservation equation can be shown in tensor form as

$$\frac{\partial}{\partial x_j}(\rho_g u_j u_i) = -\frac{\partial P}{\partial x_i} + \frac{\partial \tau_{ij}}{\partial x_j} + S_{ui} + S_{F_i} \tag{4}$$

where S_{ui} in Eq. (3) contain source representing momentum exchange between the water droplets and the surrounding gas and in a rotating frame of reference, also including appropriate contributions to represent Coriolis and centripetal forces. S_{ui} is defined as

$$S_{ui} = -S_\alpha u_i \tag{5}$$

S_{F_i} contains the smaller terms from the gradient of the Reynolds stress tensor. In general, for compressible turbulent flow S_{F_i} is

$$S_{F_i} = \frac{\partial}{\partial x_j}\left[\mu_{eff}\left(\frac{\partial u_i}{\partial x_i} - \frac{2}{3}\delta_{ij}\frac{\partial u_k}{\partial x_k}\right)\right] \tag{6}$$

In the last equation, δ_{ij} is Kronecker delta function and μ_{eff} is the effective dynamic viscosity (laminar and turbulent dynamic viscosity).

As mentioned before, droplets have very fine radius, so the assumption of elimination of drag force between two phases could be acceptable. Therefore, the momentum equation for liquid phase has been dissolved.

3. Energy Equations

The conservation of total energy for vapor phase as total enthalpy, H_g, with source term of S_h that contains the interphase heat transfer is in the form of

$$\frac{\partial}{\partial x_j}(\rho_g u_j H_g) = -\frac{\partial q}{\partial x_j} + \frac{\partial}{\partial x_j}(u_i \tau_{ij}) + S_h \tag{7}$$

H_g equals to $h_g+\frac{1}{2}u_iu_i+\kappa$ where h_g is the vapor specific enthalpy and κ is the turbulent kinetic energy. For a rotating frame of reference the rothalpy, I_g, that is $H_g-\omega^2R_\omega^2/2$ is advected instead of H_g. The energy conservation equation for high speed flow contains a term of viscous work and viscous dissipation that are shown as the second term of the right side expression of Eq. (7). In this term τ_{ij} is the viscous stress tensor. Also, S_h contains the interphase heat transfer described as below:

$$S_h = -S_\alpha h_p \tag{8}$$

where h_p is the enthalpy of liquid droplets.

The temperature of the droplets can be determined by capillarity effect, and since the droplets have very small size, their temperatures are assumed uniform through the droplets. With the definition of T_s as the saturation temperature at the local pressure, P, the temperature equation for water droplet can be shown as

$$T_{droplet} = T_s(P) - [T_s(P) - T_g]\frac{r^*}{\bar{r}} = T_{supercool}\frac{r^*}{\bar{r}} \tag{9}$$

where r^* is the critical droplet radius that will be described subsequently.

4. Nucleation

Very fine spherical droplets can be formed when a free-energy barrier to forming such droplets is overcome [3]. At large levels of supercooling, for steam in the range of 30-50 K depending on expansion rate, enough droplets are able to appear. The heat and mass transfer between the released dispersed droplets and its vapor brings the flow back to near equilibrium conditions. At these high levels of supercooling the critical droplet radius is very small given by the Eq. (10).

$$r^* = \frac{2\sigma}{\rho_l \Delta G_g} \tag{10}$$

Where σ is the water surface tension that will be described later and is the bulk Gibbs free energy change of the gas phase that de-

pends on the equation of state and will be described in the thermodynamics properties section. The equation for droplet number can be defined as

$$\frac{\partial}{\partial x_j}(\rho_g u_j N) = J \tag{11}$$

In this equation J is the number of droplets formed that is obtained from classical nucleation theory (nucleation rate [#/m^3 s]) [8]. With defining q_C as a condensation coefficient and η would be complemented (Eq. (12)). Where γ is the specific heat ratio (average value for γ of superheated steam equal to 1.32 has been used throughout this study [9]) and is the equilibrium latent heat. The gas constant and temperature of gas are R, and T_g respectively. m is the mass of one water molecule and K is Boltzmann's constant. With these assumptions J could be defined as Eq. (13).

$$\eta = 2\frac{\gamma-1}{\gamma+1}\frac{h_{fg}}{RT_g}\left(\frac{h_{fg}}{RT_g}-0.5\right) \tag{12}$$

$$J = \frac{q_C}{1+\eta}\left(\frac{2\sigma}{\pi m^3}\right)^{0.5}\frac{\rho_g}{\rho_f}\exp\left(-\frac{4\pi r^{*2}\sigma}{3KT_g}\right) \tag{13}$$

5. Thermodynamics Properties of Water and Steam

For modeling the thermodynamics properties of water and steam and surface tension of water in numerical solution, the equations of IAPWS (International Association of Properties of Water and Steam) are applied. A comparative analysis between the computational implementation of the industrial formulation of the thermodynamic properties of water at liquid and steam phases, proposed by the International Association for the Properties of Water and Steam, known as IAPWS-IF97 and other models based on foregoing propositions, from an application on Rankin cycle shows IAPWS's accuracy [6]. For transport properties of water and steam, as dynamic viscosity and thermal conductivity, the equations of ideal and real parts of fluid are employed [10]. Surface tension between liquid and vapor phase in the range of validity, from the triple point to the critical point of water and steam curve, is

$$\frac{\sigma}{1\ \mathrm{mNm^{-1}}} = 235.8(1-\theta)^{1.256}[1-0.625(1-\theta)] \tag{14}$$

where $\theta = T/T^*$ and $T^* = T_c = 647.096$ K.

6. Numerical Solution Methodology

This approach involves discretizing the spatial domain into finite control volumes. According to the supersonic flow at the nozzles, fine meshes successive ration of 1.05 at the throat are applied. The minimum volume of grids is 3.2×10^{-11} m^3 and maximum volume is 1.1×10^{-10} m^3. The numbers of nodes through the length of nozzles are 500 and for width of them, from wall to middle axis, are 60. Results of simulation with these meshes have the reasonable differences from lesser size meshes. The governing equations are integrated over each control volume, such that the relevant quantity (mass, momentum, energy, etc.) is conserved in a discrete sense for each control volume. It is clear that each node is surrounded by a set of surfaces that defines the control volume. All the solution variables and fluid properties are stored at the element nodes. Considering the mean form of the conservation equations for a general scalar of ϕ in Cartesian coordinates is

$$\frac{\partial}{\partial x_j}(\rho U_j \phi) = \frac{\partial}{\partial x_j}\left(\Gamma_{eff}\left(\frac{\partial \phi}{\partial x_j}\right)\right) + S_\phi \tag{15}$$

This equation is integrated over a control volume, and Gauss' divergence theorem is applied to convert volume integrals to surface integrals. If control volumes do not deform in time, then the time derivatives can be moved outside of the volume integrals and the equation becomes

$$\frac{d}{dt}\int_V \rho\phi dV + \int_S \rho U_j \phi dn_j = \int_S \Gamma_{eff}\left(\frac{\partial \phi}{\partial x_j}\right)dn_j + \int_V S_\phi dV \tag{16}$$

where V and s, respectively, denote volume and surface regions of integration, and dn_j is the differential Cartesian components of the outward normal surface vector. The volume integrals represent source or accumulation terms, and the surface integrals represent the summation of the fluxes [11]. Both vapor and liquid phase conservation equation are discretized using conservative finite volume integration over a control volume. The discretization of the vapor phase equation, in the context of a finite element representation of the geometry, is as follows for a general scalar ϕ,

$$\sum_{ip}\dot{m}_{ip}\phi_{ip} = \sum_{ip}\left(\Gamma_\phi\frac{\partial \phi}{\partial x_j}\Delta n_j\right) + S_\phi V_{CV} \tag{17}$$

where $\dot{m}_{ip} = (\rho u_j \Delta n_j)_{ip}$ and V_{CV} is the volume of the control volume, the subscript ip denotes an integration point, the summation is over all the integration points of the surface, and u_j is the velocity vector. Fig. 2 shows a typical mesh with unit depth, on which one surface of the control volume is represented by the shaded area. The source terms relevant to condensation and evaporation for the momentum and liquid scalar equations are applied over the control volume, and

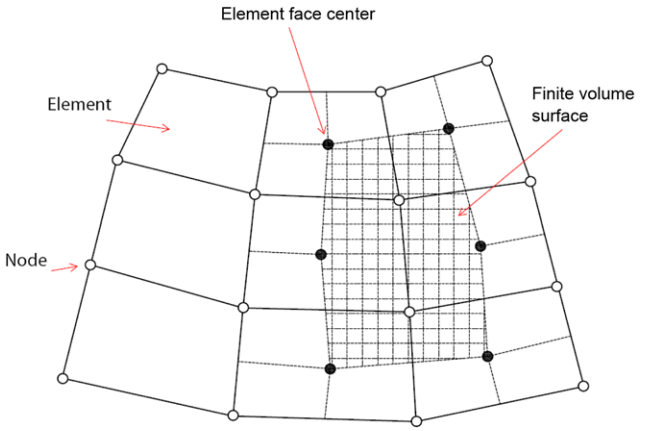

Fig. 2. The location of finite volume faces and elements.

Table 1. Boundary conditions

	Inlet			Outlet
	P_0	T_0	Wetness fraction	
Nozzle S	28.6 bar	530.3 K	0.00	Supersonic
Nozzle M	28.6 bar	536.1 K	0.00	Supersonic
Nozzle L	28.6 bar	543.7 K	0.00	Supersonic

can be linearized into passive and active terms to promote convergence of the discrete equation set [3,4]. Tests have been run within the commercial CFD code ANSYS-CFX 11.

As mentioned before, in this paper three different supersonic nozzles are used to be under simulation. Total pressure and total temperature for inlet with water mass fraction of zero and supersonic outflow for outlet are applied as boundary conditions. Ten tests have been run for these nozzles. Three of them are chosen to bring their results as follows. Values for boundary conditions of these three tests are in Table 1.

7. Validation

To validate the simulation, the calculated pressure and droplet size profiles of three tests are compared with the experimental data [1] and good agreements have been observed. Fig. 3(a)-(c) shows

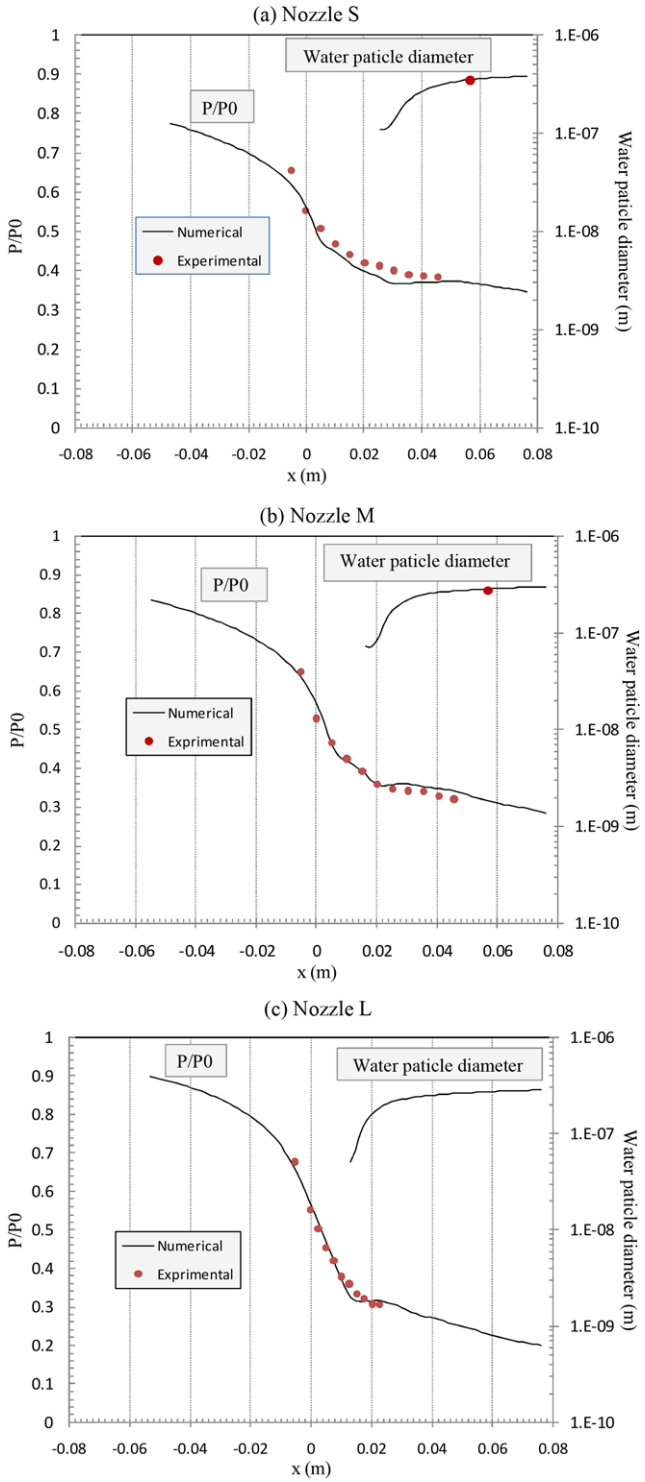

Fig. 3. Numerical data vs. experiments.

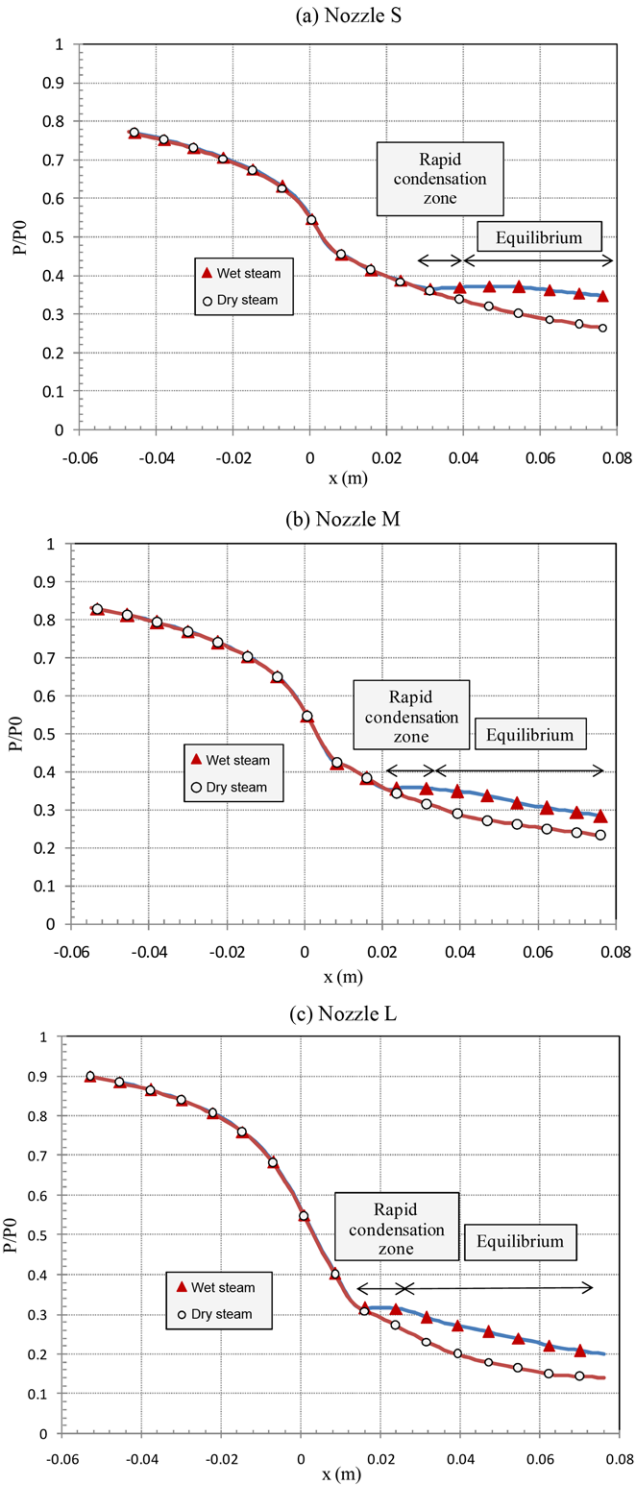

Fig. 4. Wet steam pressure profile vs. dry steam.

these correspondences.

In these figuresthe horizontal axis stands for axial distance of nozzles, x (m), the position of zero represents the throat of nozzles. Negative value of x is for the divergence part and positive value is for the convergence part of nozzles. The right vertical axis in Fig, 3(a)-(c) is overall pressure ratio (P/P_0) and the left one represents water particle diameter (m) on the middle of the nozzle.

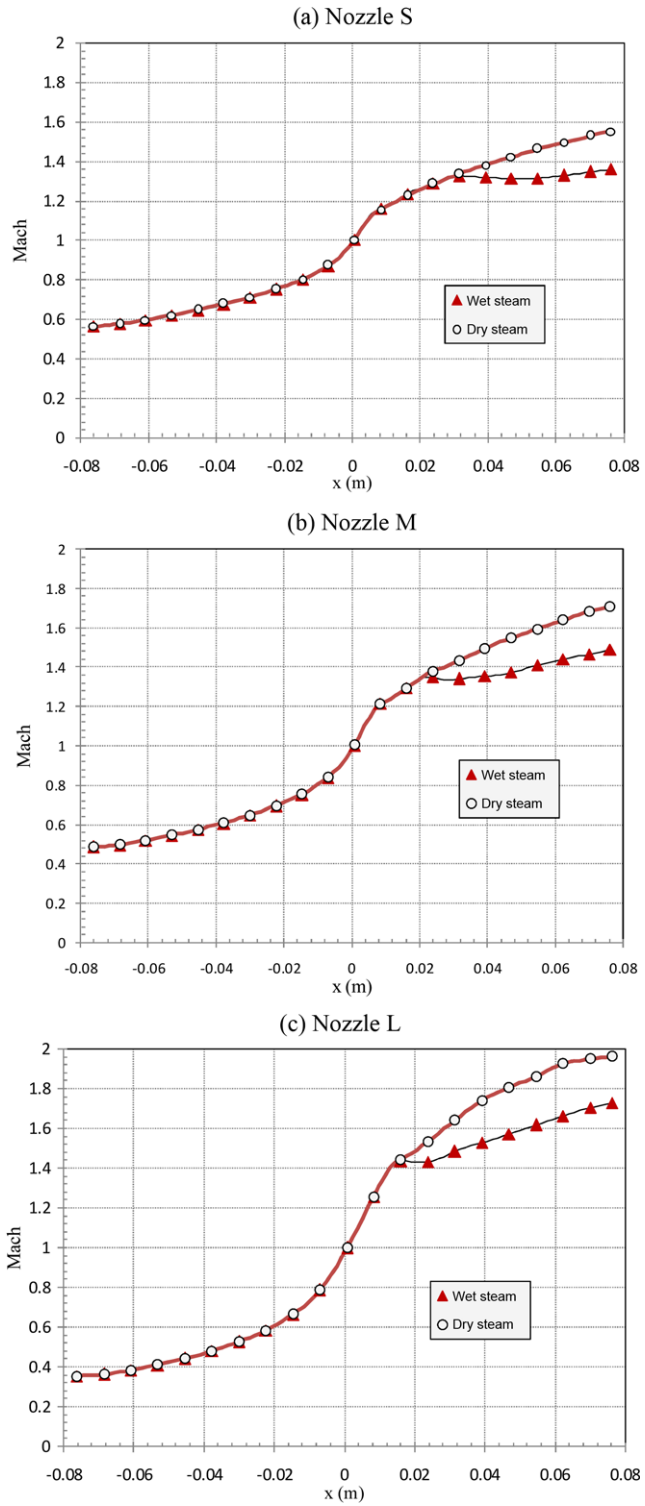

Fig. 5. Wet steam Mach number vs. dry steam.

RESULTS

As is clear from the particle diameter curve in Fig. 3(a)-(c), the appearance of droplet begins at the beginning of the convergence part. In nozzle L, that has the greatest rate of expansion, the position

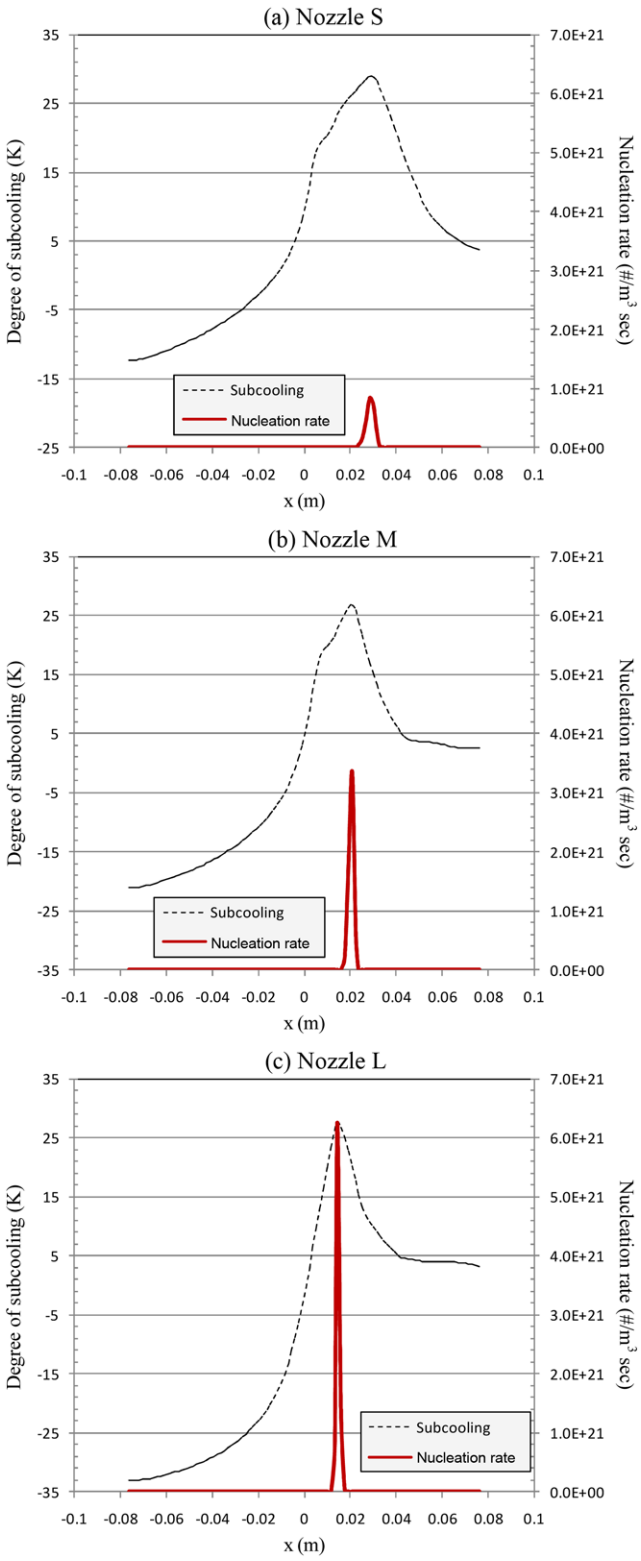

Fig. 6. Subcooling and nucleation rate.

of occurrence of nucleation is nearer to the throat, and so, for nozzle S, this position is the farthest from the throat. After the nucleation phenomenon and formation of very fine droplets, the particles grow immediately and then their rate of growth becomes lower. In Fig. 4(a)-(c) the pressure profiles for three mentioned tests and also three other tests with the same pressure conditions at inlet, but 40 °K higher total temperature in this area, are drawn. In other words, the cases in the second test group are dry steam without nucleation.

Comparison of the droplet and isentropic (dry steam) pressure curves specifies that the wet steam pressure profile in the nucleation position does not comply with the isentropic manner and within a rapid condensation changes the pattern of pressure drop. After equilibrium of first and second phases, the wet steam pressure profile drops similarly to dry steam. This position of equilibrium is near to the location where the growth rate of droplet sizes becomes low in Fig. 3.

During the expansion within the wet steam, decreasing the temperature is quicker than the saturation temperature at the same pressure. Therefore, the metastable supercool or super saturation condition governs the domain. With an adequate level of supercooling (Fig. 6) that is defined as differences of the local temperature and saturation temperature at the same local pressure, nucleation occurs and very fine clusters of droplets form and then with a rapid condensation, the condition will be brought back to equilibrium. These events and effects of them on pressure profile are shown in Fig. 4. Releasing of latent heat and transferring it from droplets to the gas phase results in condensation shock that raises the pressure locally [12] (Fig. 5). This condensation shock also has effects on the Mach number, as can be seen in Fig. 5(a)-(c). The flow is supersonic in the diverging portion of the nozzle, with deceleration of the flow through the nucleation zone.

In Fig. 6(a)-(c) degree of subcooling and the nucleation rate (J [#/m^3 sec]) that has been described former is shown. From this figure, it is clear that in the location with the highest degree of subcooling, the highest nucleation rate occurs. Also just at this location the second phase appears and after that degree of subcooling and nucleation rate decreases with the equilibrium of the system.

After nucleation, the number of droplets suddenly increases and rises to order of 10^{16} and remains at this order. In Fig. 7 the water droplet number at the middle axel of nozzles with the right vertical axis and water mass fraction in this location with the left vertical axis are shown. In these figures, also the water mass fraction though the nozzles is shown. As mentioned, the rate of increasing the size of droplets, after the rapid condensation zone, decreases but the drop-

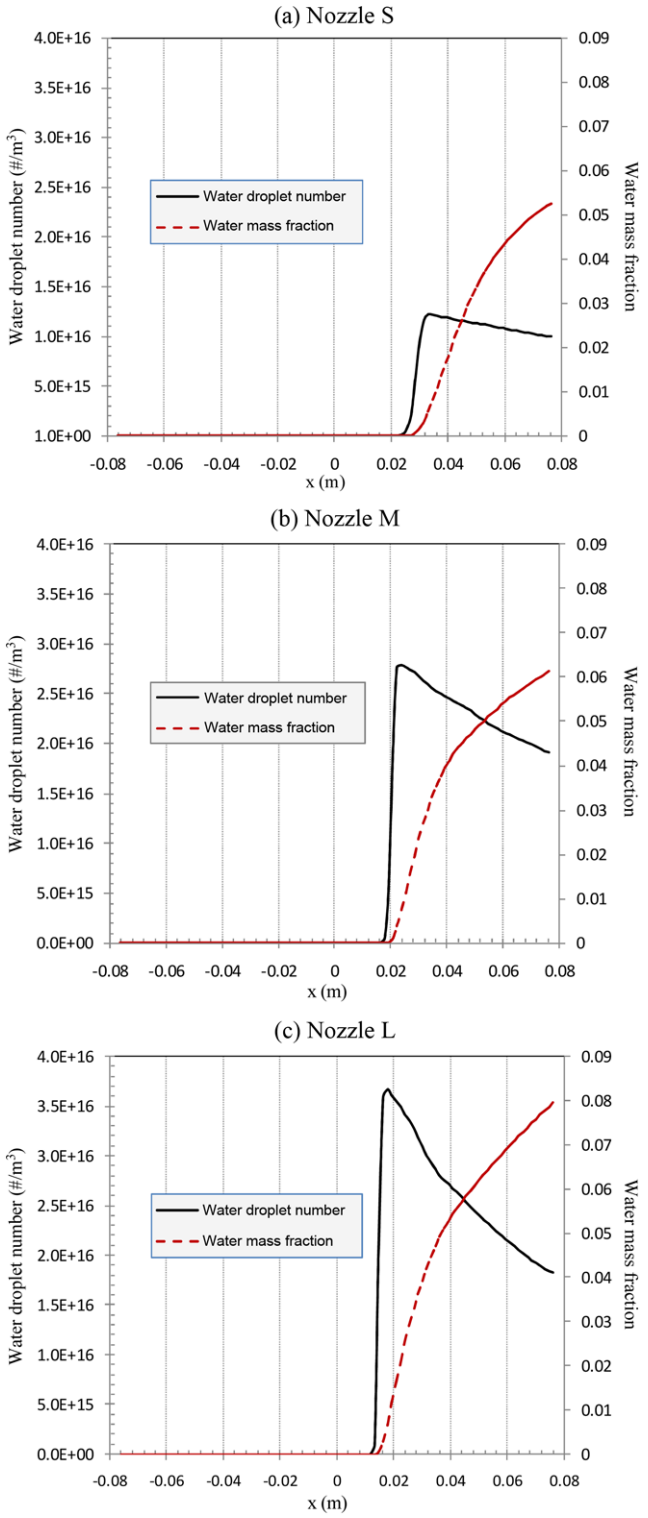

Fig. 7. Wetness fraction and droplet number.

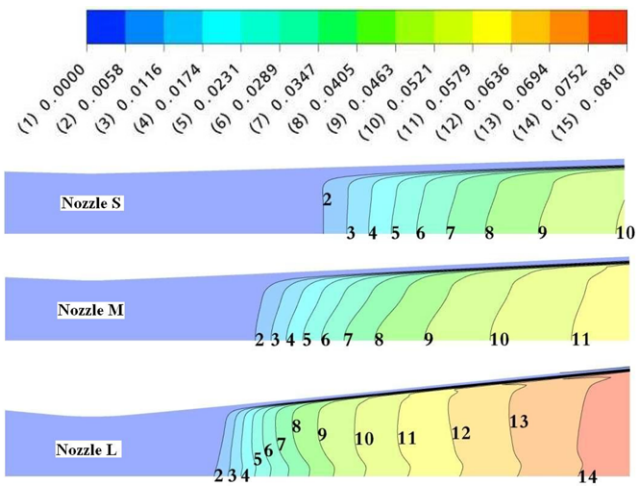

Fig. 8. Water mass fraction contours.

let size increases up to two or three times. This matter causes increasing of water mass fraction. Maximum mass fraction occurs in the nozzle with the largest rate of expansion.

In Fig. 8 water mass fraction contours during crossing the steam within nozzles are illustrated. As can be seen, in the nozzle with the highest rate of expansion, nucleation occurs nearer than to the throat and the maximum of this parameter exists at the end of this nozzle. The maximum water mass fraction for nozzle S is 0.0526 as this value for nozzles M and L is 0.0612 and 0.0807 respectively.

CONCLUSION

The most important characteristic of the two-phase steam flow with nucleation is the supercooling in steam and subsequent release of latent heat because of rapid condensation. This phenomenon causes nucleation shock that has an effect on the pressure profile. After this zone, heat and mass transfer return the system to thermodynamic equilibrium. Based on Eulerian-Eulerian multiphase numerical simulations, reasonable agreement with experimental data for pressure distribution in the three converging-diverging nozzles with different expansion ratio has been obtained. In these cases there is an overexpansion in the diverging section followed by diffusion that dominates the temperature profile and causes condensation. Within this simulation for these three supersonic nozzles, the most condensation and water mass fraction exist in nozzle L, which has the highest rate of expansion.

NOMENCLATURE

C_p : specific heat of liquid [J/kgK]
C_V : vapor isochoric specific heat [J/kgK]
h : static enthalpy [J/kg]
H : total enthalpy [J/kg]
I : rothalpy [J/kg]
J : nucleation rate [droplet #'s/m^3 s]
K : Boltzmann's constant
m : mass [kg]
N : number of droplets per unit mass of vapor [=droplet #'s/mg], droplet #'s/kg$_g$
P : pressure [N/m^2]
q_c : condensation coefficient
r : droplet radius [m]
r* : droplet critical radius [m]
R : gas constant (=461.4 J/kg K), or radius of rotation
s : static entropy [J/kg]
S : surface [m^2]
S_F : source term for momentum equation with smallest contribution from viscous gradients [N/m^3]
S_α : source term representing the condensation rate of vapor [kg/m^3 s]
S_ϕ : source term of a general scalar equation
t : time [s]
T : temperature [K]
T_C : critical temperature [K]
T* : critical temperature [K]
u : velocity [m/s]
V : volume of a single control volume
x : spatial dimension [m]

Greek Symbols

α : mass fraction of liquid water to water vapor (=mf/mg) [kg$_f$/kg$_g$]
γ : vapor specific heat ratio
Γ : turbulent diffusion coefficient of the liquid scalar equation α kg/m s
δ : Kronecker delta function
Δn : outward unit vector of the discrete surface
Δt : time step
ΔG : bulk Gibbs free energy change [J/kg]
θ : reduced temperature
η : correction parameter
κ : turbulent kinetic energy [m^2/s^2]
μ : dynamic viscosity [kg/m s]
ρ : density [kg/m^3]
π : pi number
σ : liquid surface tension [N/m]
τ : stress [N/m^2]
ϕ : general scalar
υ : specific volume [m^3/kg]
ω : rotational velocity [radian/s]

Subscripts

B : Border line between region 2 and 3 in IAPWS
c : critical
cv : control volume
eff : effective (laminar+turbulent)
g : gas
ijk : tensor notation
ip : integration point
l : liquid
s : saturated state

Super Script

o : property evaluation at old time values

REFERENCES

1. F. Bakhtar and K. Zidi, *Proc. Inst. Mech. Eng*., **203**, 195 (1989).
2. F. Bakhtar and K. Zidi, *Proc. Inst. Mech. Eng*., **204**, 233 (1990).
3. A. G. Gerber, *ASME J. Fluids Eng*., **124**, 465 (2002).
4. A. G. Gerber and M. J. Kermani, *Heat and Mass Transfer*, **47**, 2217 (2004).
5. D. A. Simpson and A. J. White, *International J. Heat and Fluid Flow*, **26**(1), 71 (2005).
6. Equations of IAPWS-IF97, A summary by Bernhard Spang, Hamburg, Germany, at The Chemical Engineers' Resource Page.
7. IAPWS Equations for Transport Properties and, Surface Tension of Water and Steam, A summary by Bernhard Spang, Hamburg, Germany, at The Chemical Engineers' Resource Page.
8. J. E. McDonald, *Am. J. Phys*., **30**, 870 (1962-1963).
9. M. J. Kermani, M. Zayernouri and M. Saffar-Avval, *Generalization of an analytical tow-phase steam flow calculator to high-pressure cases*, Department of Mechanical Engineering, Amir Kabir Uni-

versity of Technology, Tehran, Iran.
10. IAPWS Equations for Transport Properties and, Surface Tension of Water and Steam, A summary by Bernhard Spang, Hamburg, Germany, at The Chemical Engineers' Resource Page.
11. ANSYS CFX 11-Solver Theory Guide, Discretization and Solution Theory, 227 (2006).
12. A. R. Teymourtash and M. R. Mahpeykar, A Balde to Balde Inviscid Transonic Flow Analysis of Nucleating Steam in a Turbine Cascade by the Jameson's Time - Marching Scheme Using Body Fitted Grid, Ferdosi University (2006).